electronics

MDPI

Article

Design a Compact Printed Log-Periodic Biconical Dipole Array Antenna for EMC Measurements

Abdulghafor A. Abdulhameed [1,2,*] and Zdeněk Kubík [1]

[1] Department of Electronics and Information Technology, Faculty of Electrical Engineering, University of West Bohemia, 301 00 Pilsen, Czech Republic
[2] Department of Electrical Techniques, Qurna Technique Institute, Southern Technical University, Basra 61001, Iraq
* Correspondence: abdalhme@fel.zcu.cz

Abstract: This article presents the design, modeling, and fabrication of a printed log-periodic biconical dipole array antenna (PLPBDA) for electromagnetic compatibility (EMC) measurements. The proposed structure used bow tie-shaped dipoles instead of typical dipoles to achieve a size reduction of 50% and bandwidth enhancement of 170% with the help of PCB technology. Furthermore, the balanced feeding method and the modifications in bow tie-shaped dipole dimensions were utilized to obtain broad bandwidth of 5.5 GHz (from 0.5 GHz to 6 GHz). This structure comprises 12 dipole elements with a compact size of 170 × 160 × 1.6 mm, reflecting low fluctuations gain of about (4.6–7) dBi with the help of an extra dipole. Moreover, the achieved frequency and radiation characteristics (simulated and measured) agree with each other and are compatible with the results of classical EMC antennas. The achievements of this structure showed promising results compared to both literature reviews and reference antenna Hyper LOG® 7060 offered for sale.

Keywords: antenna factor; biconical antenna; EMI; bowtie; PLPBDA; EMC measurement

Citation: Abdulhameed, A.A.; Kubík, Z. Design a Compact Printed Log-Periodic Biconical Dipole Array Antenna for EMC Measurements. *Electronics* **2022**, *11*, 2877. https://doi.org/10.3390/electronics11182877

Academic Editor: Massimo Donelli

Received: 19 August 2022
Accepted: 8 September 2022
Published: 11 September 2022

1. Introduction

With the rapid growth of wireless communications, the need to use Ultra-wideband antennas in such systems has appeared in various applications. Furthermore, the antenna design is the key to every wireless system since it can control its radiation characteristic according to the application's specifications [1]. Ultra-wideband antennas are used in different applications, e.g., in radio systems for communications and in electromagnetic compatibility (EMC) for measurement applications. The evolutions in wireless systems have motivated researchers to develop new communication forms to exploit the spectrum in the best way and enhance the reception quality [2–5]. Therefore, the cognitive radio technology was the best solution for this matter as it consists of two different antennas, one for sensing with Ultra-wideband of (3.1–10 GHz) to identify the state of the band-idle or active, while the other antenna is a communication antenna (reconfigurable antenna) [6–11]. This research focuses on the EMC applications, whereas an Ultra-wideband antenna can be used as a reference antenna for emission and immunity tests of the device under the test (DUT) inside the EMC chamber [12]. Several antenna configurations have been utilized to measure electromagnetic interference (EMI) based on the operation frequency and radiation characteristics. For instance, in [13], the authors showed the AF characteristics of the sleeve dipole antenna for EMC measurement by changing the sleeve dipole parameters, which offered an 86% size reduction compared to the conventional biconical antenna with similar characteristics. The performance of the log-periodic dipole array antenna was improved in [14] using a saw-tooth shape feedline. The successive dipoles will be arranged in the same horizontal plane, eliminating the unwanted vertical electric field component. A complimentary log-periodic dipole array with cross-polarization was proposed in [15]. This structure has a set of dipole antennas orthogonal to conventional log-periodic dipole

antennas, offering a circular polarization without any hybrid junction. A pair of printed broadband Vivaldi antennas with a coaxial feeding method operating from 0.5 GHz to 4 GHz was designed, fabricated, and tested [16]. Moreover, the proposed design served as a reference antenna for EMC measurement since it exhibited stable radiation characteristics and a maximum gain of 6.2 dBi. The width of the ridge of the double ridge guide horn (DRGH) antenna was tapered linearly in [17]. This process maximized the effective radiation aperture and reduced the beamwidth compared to conventional 1–18 GHz DRGH. Another horn antenna with miniature size and wide bandwidth was presented in [18], where the idea of extending the lower frequencies was inspired by the fishtail structure and classical ridge structure. UWB skeletal antenna was proposed in [19]. This antenna showed good results in VSWR compared with the biconical antenna in the band up to 200 MHz, which is considered another wire UWB antenna family. Ref. [20] presented a novel UWB monopole antenna for EMC measurement applications, and this antenna covered two bands (0.79–1 GHz) and (1.37–10 GHz). In Ref. [21], the authors proposed a novel method for optimizing small elliptical planner dipole antenna for ultra-wideband EMC applications. The characteristics of this antenna-like wide band (1–5 GHz) and flatness gain enabled it to be a powerful tool for EMC measurements. The LPDA antenna is extensively used because it provides a high directivity and flat gain over the wideband spectrum [22].

Moreover, an LPDA antenna is called frequency-independent when the ratio of higher frequency to the lower frequency is more than ten times, where the impedance and radiation characteristics remain constant as a function of frequency. The lower operating frequency of the LPDA determines its size and, consequently, the length of the most extended dipole. Since the aimed wide operation frequency band starts from 500 MHz, the LPDA length will be considerably large. To overcome this LPDA size limitation, the printed log-periodic dipole array (PLPDA) antenna has been presented recently utilizing printed circuit board (PCB) technology that offers good specifications such as low cost, low profile, small size, and easy fabrication [23]. In PLPDA, all the parameters of the conventional LPDA antenna are divided by the square root of the effective dielectric substrate ($\sqrt{\varepsilon_{eff}}$).

The majority of EMC reference antennas are dedicated to serving in the band starting from 700 MHz to 2.4 GHz since this band is occupied by different applications such as GSM 850–900 MHz, mobile 1800 MHz, 3G 2100 MHz, and Wi-fi 2400 MHz and has a high probability to interference [24]. On the other hand, the band from 2.5 GHz to 6 GHz must be taken into account due to the fact it is occupied with another set of critical applications such as WiMAX 3.5 GHz and 5.3 GHz, mid bandwidth for 5G 2.5–3.8 GHz, PAN 4.8 GHz, and WLAN 5.8 GHz [25].

In the last decade, several structures of PLPDA serving different applications were presented; some offer size reduction, while others provide wide bandwidth. For instance, Casula et al. [26] showed an ultra-wideband (4–18 GHz) printed log-periodic dipole array antenna design with 15 dipoles. An infinite balun was realized using two symmetrical coaxial cables attached at the top and bottom sides. Moreover, this antenna was designed to stabilize its radiation pattern without changing the phase center during the operating band. Step-by-step design procedures for PLPDA antenna were illustrated in [27]. The design started with nine dipole elements according to the spacing and scaling factor values of 0.78 and 0.14. Then, three extra dipoles were added to satisfy the condition ($S11 < -10$ dB) through the whole operation band. Therefore, this antenna offered wide bandwidth starting from 800 MHz to 2.5 GHz with size reduction using only 12 dipoles. In [28], a PLPDA antenna with a balanced feed structure was presented. The authors modified the width of the feeding lines to compensate soldering effect and offer broadband impedance bandwidth starting from 500 MHz to 3 GHz. Furthermore, a stable high gain with low tolerance of 0.5 dB was achieved. In [29], 48 dipole elements were utilized to obtain wide bandwidth of 8.5 GHz using the hat-loaded technique for the first three dipoles and the technique of T-shaped loaded for the following three dipoles. Moreover, wide impedance bandwidth was achieved using meandered line and trapezoid stub methods. Another wideband PLPDA structure (0.5–10) GHz with 25 dipole elements was presented in [30]. Wide bandwidth and

size reduction were achieved using dual-band dipole technology. Ref. [31] offered PLPDA of (0.8–2.5) GHz bandwidth using 12 dipole elements with a small size. These 12 dipoles were arranged in a way so that the length of each one decreases gradually relative to the next one, and each dipole resonates at its center frequency to cover the overall EMC spectrum L-band. A wideband printed LPDA antenna (0.4 GHz to 8 GHz) was proposed in [32]. The low-frequency response of this structure was improved by replacing the most extended traditional dipole with a triangular shape and optimizing the width, length, and spacing of the following four dipoles. The upper-frequency range of the proposed PLPDA antenna in [33] was increased to operate from 780 MHz up to 18 GHz by introducing a ratio factor parameter that used the truncate method to improve the properties of this antenna.

One of the motivations for using a compact PLPDA antenna rather than the classical one in EMC measurement is the shorter measurement distance. The shorter measurement distance can achieve a high strength field in the uniform field area (UFA) without increasing the input power in the radiated immunity test. Furthermore, radiation emission and radiation immunity are essential criteria for EMI measurements and should be performed in the far-field region. Figure 1 depicts the EMC measurements setup according to CISPR standards. The radiation pattern of the reference antenna must cover the device under the test to obtain a proper response. Usually, the devices under the test have different dimensions. Therefore, other reference antennas are required to obtain the maximum field strength. Unfortunately, having many antennas in one EMC laboratory is not the right choice. The alternative solution is to have a small number of reference antennas. The maximum field strength is achieved by changing the measurement distance according to the device under the test. Therefore, the compact antennas are fit with changing the test distance since the DUT is still in the far-field region of these antennas [34].

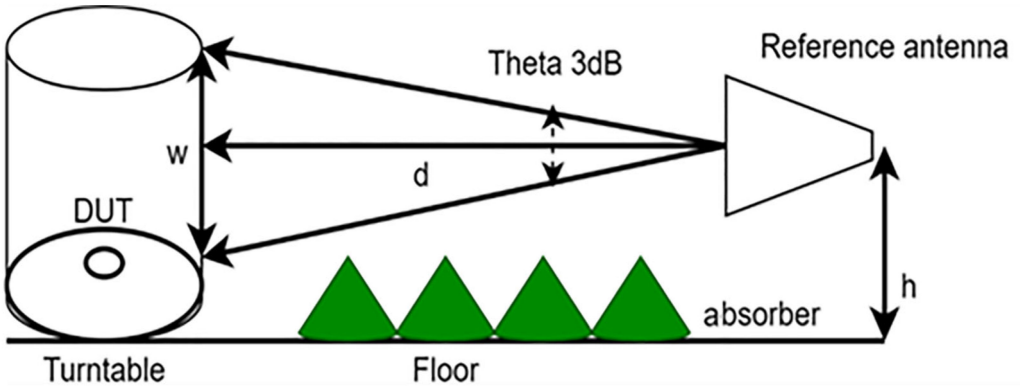

Figure 1. The EMC measurements chamber according to the CISPR standards.

The minimum measurement distance is controlled by the largest dimension of the antenna (D), DUT dimension, and the maximum resonance frequency (above 1 GHz) according to CISPR 16-1-2 [35]

$$d = \frac{D^2}{2\lambda} \quad (1)$$

Let us compare the classical log periodic dipole array antenna, which has the highest dimension, D = 340 mm, with the compact antenna having D = 170 mm. Both antennas are operating up to 6.5 GHz. According to (1), the shorter measurement distance for the classical antenna should be $ds \geq 3$ m. On the other hand, the minimum measurement distance for the proposed antenna should be $ds \geq 0.6$ m, while it must be ≥ 1 m according to CISPR standard [35]. Due to the compact size of the proposed antenna, the measurement distance (ds) could be alternated to 1.25 m in the case of small DUTs, and in this case, the illumination area will be 1.5 m, making it suitable for most DUTs.

The other motivation is the test configuration issue. Based on EMC standards, i.e., CISPR 16-2-3, the minimum distance between the reference antenna and the ground

plane must not exceed 25 cm. The main problem will occur through the test with the vertical orientation of the antenna, where the antenna will be very close to the ground, especially at low frequency. This problem will lead to wrong measurements due to interference between the reference antenna and the ground plane [36]. This problem will not be an issue in the printed reference antenna due to the small size they have by using a substrate with high relative permittivity $\varepsilon_r = 4.3$ to minimize the size, and hence, it satisfies the condition even with low frequencies. This paper presents an analytical study for a small-size printed log-periodic dipole array antenna based on bow tie-shaped dipoles instead of the typically printed dipoles. This structure aims to tackle both goals—bandwidth enhancement and size reduction—to serve as a reference antenna in EMC measurements for the band starting from 0.5 GHz to 6.5 GHz. Section 2 describes the comparative analysis of conventional and bow tie-shaped dipoles. The basic design of the log-periodic antenna is illustrated in Section 3. Section 4 briefly discusses the various feed techniques and their effect on the antenna characteristics, while Section 5 demonstrates the simulation and measurement results by comparing the literature reviewed and the proposed design. Finally, Section 6 presents a comprehensive conclusion with recommendations.

2. Comparative Analysis of Conventional and Biconical Dipoles

This section focuses on the benefits of using a biconical dipole instead of a classical one. The size reduction and bandwidth enhancement benefits have been demonstrated by designing and simulating two dipoles—conventional dipole and biconical dipole—using CST Microwave studio with a discrete feeding port, as shown in Figure 2. Furthermore, both dipoles have a length of (L = 170 mm) and widths (w1 = 6 mm and w2 = 16 mm, respectively). The proposed structures are based on an FR-4 substrate with a size of Ls = 180 mm and Ws = 160 mm.

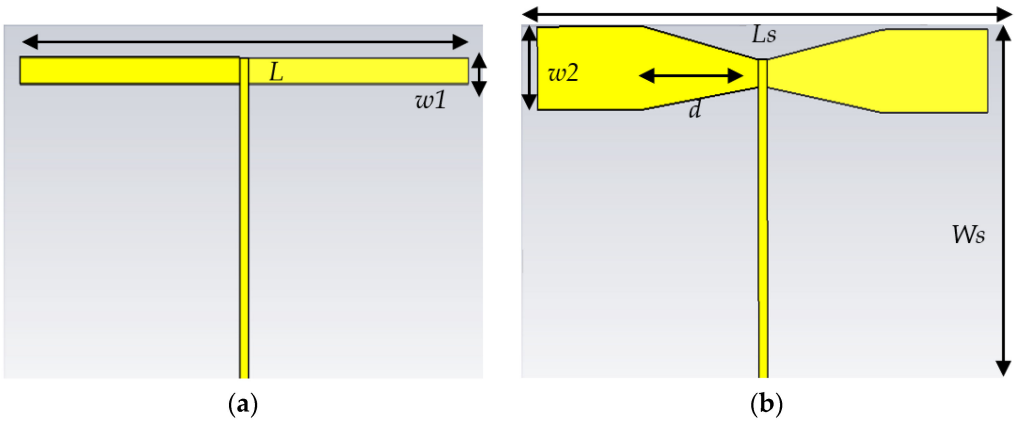

Figure 2. Two dipoles are modeled in CST Microwave Studio: (**a**) conventional dipole; (**b**) biconical dipole.

Figure 3 shows the reflection coefficient in dB versus frequency. It is clear that the proposed dipole requires a length less than a conventional one to achieve the same resonance frequency, and this process will develop by using an array of these dipoles. Moreover, the proposed dipole offers wider bandwidth than the traditional one, as is evident in the biconical dipole impedance curve in Figure 4, which is flatter with frequency than the conventional dipole curve. Figure 5 shows the role of dimension *d* in mm for tuning the bandwidth of the biconical antenna. This feature is valuable in the following design steps to obtain the optimum dimensions of the PLPDA antenna. It can be concluded that keeping the starting points of the electromagnetic waves close to each other directly impacts broadening the bandwidth [1], which is why the biconical dipole has wider bandwidth than the conventional one.

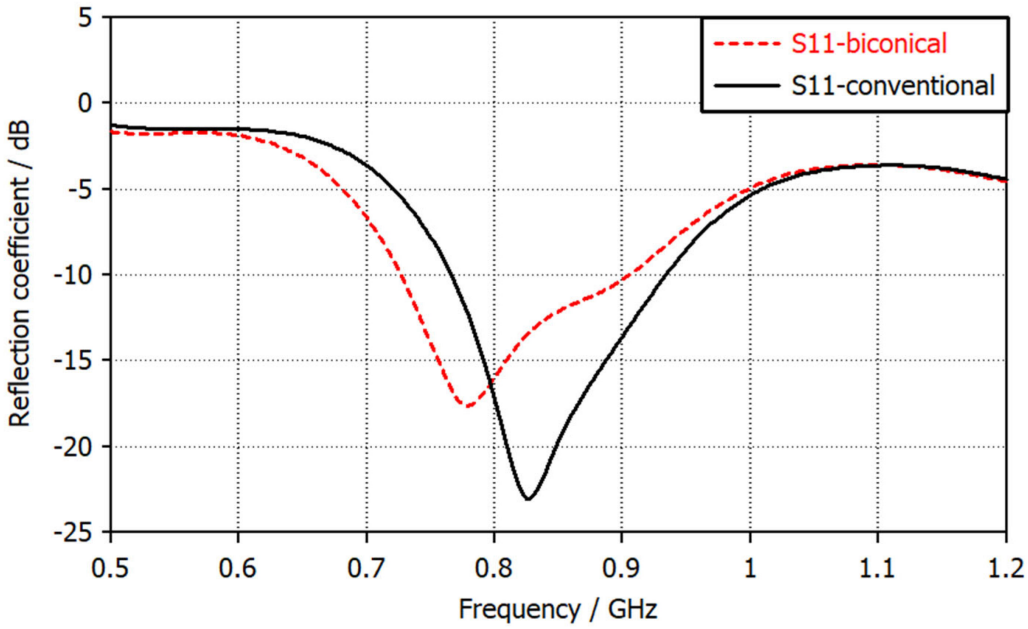

Figure 3. Reflection coefficient versus frequency for conventional and biconical dipole.

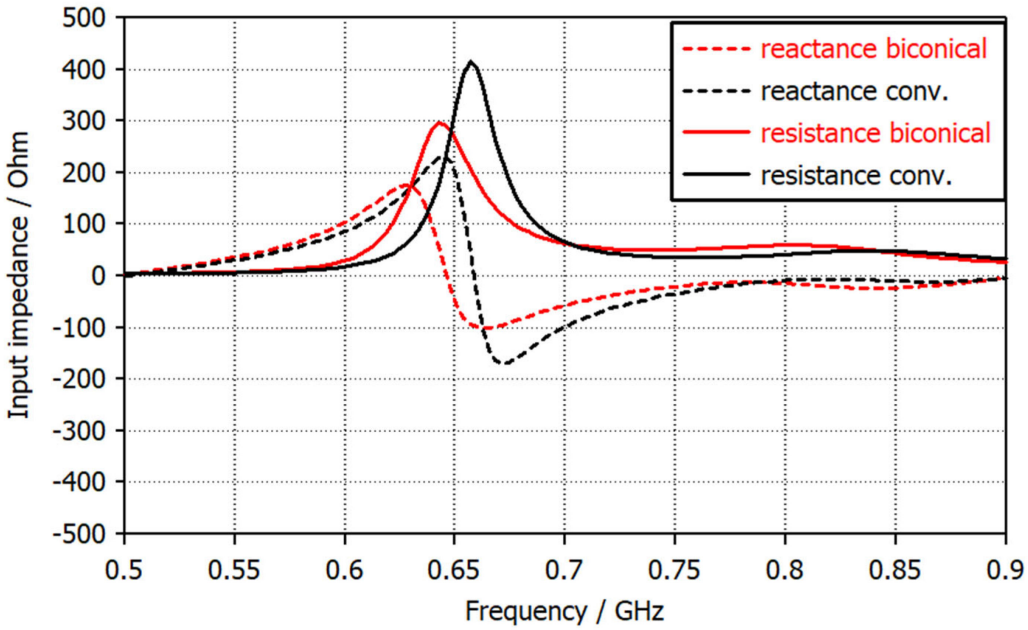

Figure 4. Input impedance versus frequency for conventional dipole and biconical dipole.

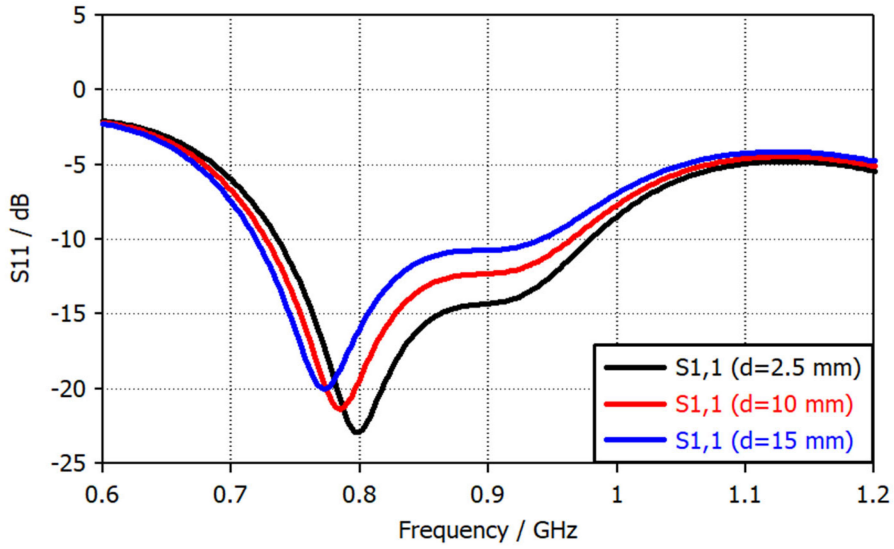

Figure 5. S11-parameter versus frequency for different values of d in mm.

3. Printed Log-Periodic Dipole Array Antenna Design

The log-periodic dipole antenna was first derived from the conventional dipole (radiate at half wavelength) by Isbell [37]. It consists of several dipoles, and each one resonates at its wavelength corresponding to the length. It is worth mentioning that all dipoles whose lengths are higher than wavelength act as reflectors, whereas they would act as directive dipoles if their lengths are smaller than the wavelength [38]. Moreover, the classical analysis method was described by Carrel [39], which presents straightforward procedures for the design using the following six steps:

1. According to the desired directivity, scaling factor (τ) and spacing factor (σ) can be evaluated from the point intersection of the straight line $\sigma = 0.243\ \tau - 0.051$.
2. Using Equations (2)–(4) to find out the maximum number of dipoles

$$N = 1 + \frac{\log B_S}{\log \frac{1}{\tau}} \tag{2}$$

$$B_S = B \cdot B_{ar} = \frac{f_{upper}}{f_{lower}} \times B_{ar} \tag{3}$$

$$B_{ar} = 1.1 + 7.7(1-\tau)^2 \frac{4\sigma}{1-\tau} \tag{4}$$

where B_S and B_{ar} present the structure bandwidth and the active region bandwidth, respectively.

3. The length of the most extended dipole (first one), which matches the lowest frequency, can be found from Equation (5).

$$L_1 = \frac{1}{2} \times \frac{3 \times 10^8}{f_{lower}} \tag{5}$$

4. The distance between each successive dipole can be calculated using Equation (6).

$$R_1 - R_2 = \frac{L_1 - L_2}{2} \times \frac{4\sigma}{1-\tau} \tag{6}$$

5. The dipoles' width can be evaluated using Equations (7) and (8).

$$Z_0 = \frac{377}{\pi}\left(\ln\left(\frac{L_n}{a_n}\right) - 2.25\right) \tag{7}$$

$$W_n = \pi \times a_n \tag{8}$$

6. Equations (9)–(11) are used to calculate the length, distance, and width of successive dipoles.

$$L_{n+1} = \tau \times L_n \tag{9}$$

$$R_{n+1} = \tau \times R_n \tag{10}$$

$$W_{n+1} = \tau \times w_n \tag{11}$$

Finally, the length of the dipoles, the width of the dipoles, and the spacing between dipoles should be divided by the square root of the effective dielectric constant, $\frac{L_n}{\sqrt{\varepsilon_{eff}}}$, $\frac{W_n}{\sqrt{\varepsilon_{eff}}}$, and $\frac{R_n}{\sqrt{\varepsilon_{eff}}}$, respectively [32]. The effective dielectric constant is described by Equation (12).

$$\varepsilon_{eff} = \frac{\varepsilon_r + 1}{2} + \frac{\varepsilon_r + 1}{2}\left[1 + 12\frac{h}{w}\right]^{-\frac{1}{2}} \tag{12}$$

According to the EMC measurement application, low bandwidth and large size were the main issues in designing printed log-periodic antennas. Using an antenna as a reference in EMC measurements requires wide bandwidth to cover the electromagnetic interference (EMI) with the communications bands that spread in the whole spectrum. On the other hand, the size was a considerable impact factor in the shorter measurements distance and test configuration. Therefore, the classical dipole elements were replaced with a trapezoidal shape to form a biconical array antenna instead of the typical dipole array since the biconical antenna offered a wider bandwidth than a classical dipole antenna [40]. By doing so, the proposed design has achieved both bandwidth improvement and size reduction simultaneously. The geometrical shapes for both conventional and biconical dipole array antennae are presented in Figure 6.

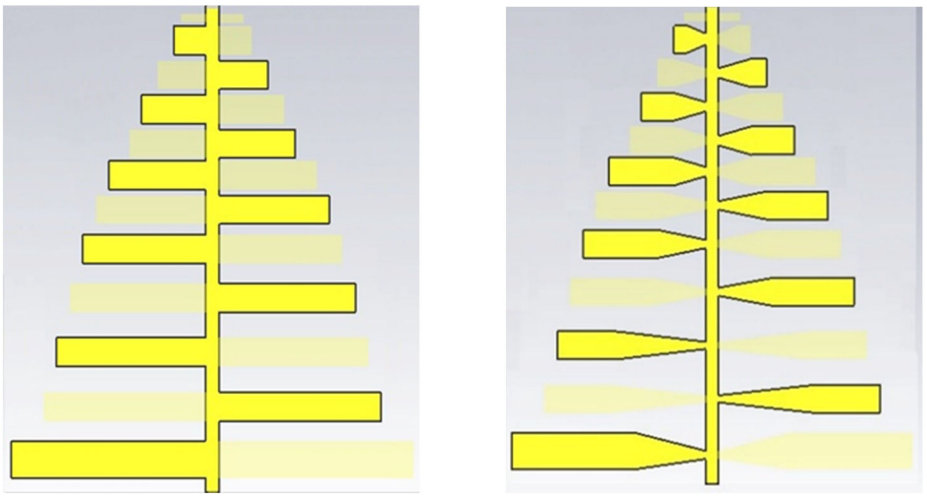

(**a**) (**b**)

Figure 6. The geometrical structure of 11 elements of (**a**) conventional design and (**b**) proposed design.

The spacing between adjacency dipoles becomes smaller as it approaches the high-frequency dipoles. In contrast, low frequencies at the longest dipoles have higher bandwidth than the lowest length dipoles, which have sharp bands. Therefore, the spacing should be obtaining small to make these sharp bands close to each other, and consequently, it leads to achieving a wide band. Figure 7 shows the reflection coefficient of the conventional and proposed designs. The biconical dipoles have significantly impacted the impedance bandwidth (from 0.5 GHz to 5.5 GHz) compared with linear dipoles (from

0.7 GHz to 3.3 GHz). Hence, the biconical dipoles have better performances than the conventional dipoles.

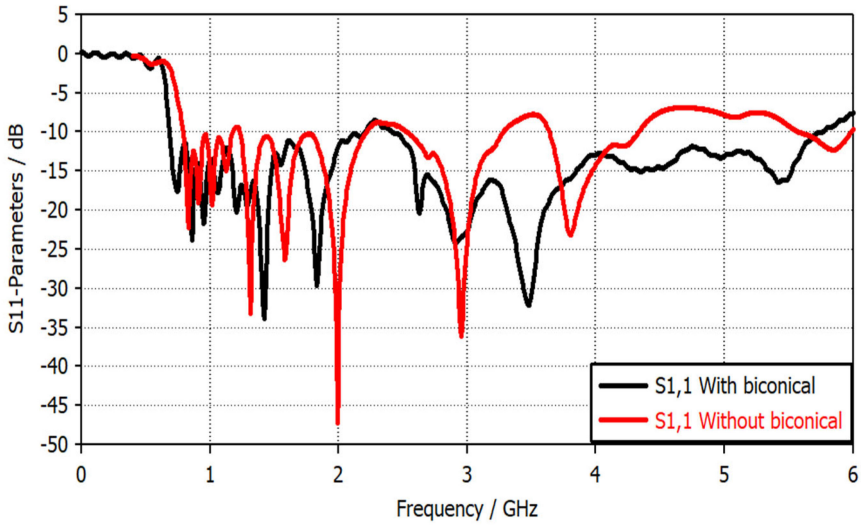

Figure 7. S11-parameter versus frequency with/without biconical structure.

Even with this promising result of the reflection coefficient of biconical dipoles array antenna, the voltage standing wave ratio still does not satisfy the condition VSWR < 2, especially at 2.4 GHz, in which the reflection coefficient is approximate −9 dB. Hence, an extra dipole (conventional one) is designed and optimized to eliminate this reflection, and the result is shown in Figure 8. This additional dipole was inserted between the input port and the biconical element number 11 [27]. It is clear that through the whole frequency band from 0.5 GHz to 6 GHz, the VSWR < 2, and the reflection coefficient value is now below −10 dB. Furthermore, it was found that the changing of the extra additive dipole length has also significantly affected the gain values. Figure 9 presents the gain variation with different lengths of this extra dipole. The length $L12$ = 10 mm reflects the lowest gain fluctuations, which is necessary to achieve a good antenna factor result with low uncertainty. However, the gain could be flatter with increasing the length of the additive dipole, but it will corrupt the impedance matching since there is a trade-off process. Therefore, $L12$ = 10 mm is the optimum value for both the s-parameter and the gain.

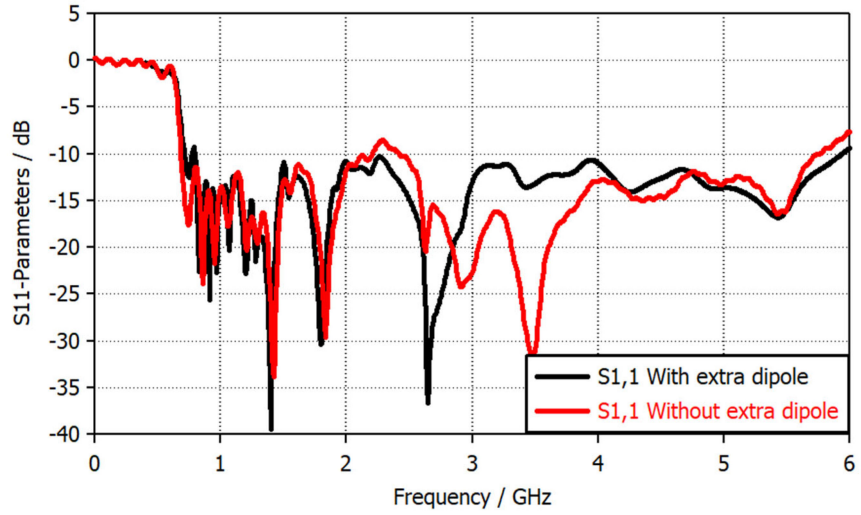

Figure 8. S11-parameter versus frequency with/without extra dipole.

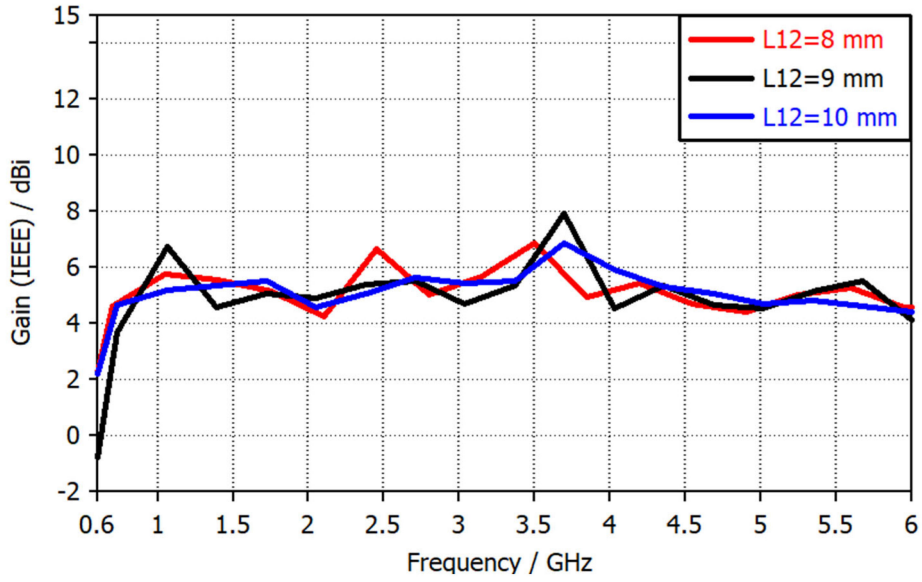

Figure 9. Simulated gain with different lengths of extra dipole.

Figure 10a shows the optimized geometrical shape of the design, while Table 1 illustrates the optimum values of each dipole element's parameter. The width of the dipole is set at the value of 10 mm except for the first dipole's width ($W1$ = 13 mm) and the extra dipole's width ($W12$ = 5 mm). On the other hand, parameter (d) plays a vital role in having broadband impedance matching since it is the central part of modifying every dipole's biconical shape, as shown previously in Figure 5. Finally, an optimization process took place on the overall dimensions to obtain better performances using Microwave CST Studio's facilities [41]. The utilized structure is epoxy FR-4 relative permittivity $\varepsilon_r = 4.3$, and loss tangent of $tan\delta$ = 0.025. Figure 10b depicts the cross-section area of the proposed structure.

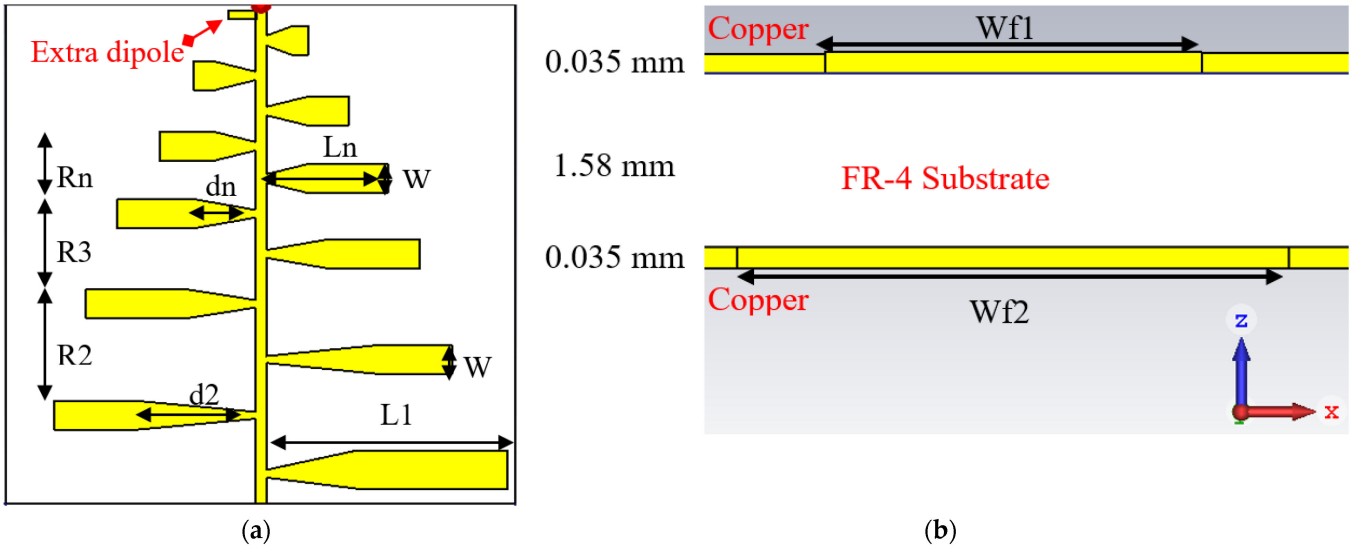

Figure 10. (**a**) The optimized structure of the biconical dipole array antenna; (**b**) cross-section area for the biconical dipole array antenna.

Table 1. Illustration of optimum values of the parameters.

No.	1	2	3	4	5	6	7	8	9	10	11	12
L (mm)	77.5	65	60	55	50	45	40	31.8	27.5	21.2	15	10
W (mm)	13	10	10	10	10	10	10	10	10	10	10	5
R (mm)	20	19	19	17	13.7	12	12	12	12	12	12	–
d (mm)	20	30	27.5	13.75	11.25	11.25	11.25	5	5	5	5	–

4. Feeding Techniques

The feeding techniques play a vital role in designing the log-periodic dipole antenna array. The typical feeding method consists of two non-radiated microstrip lines attached to each substrate's side to connect the successive dipoles. There will be a 180° phase difference between every two consecutive dipoles, ensuring the energy will radiate only from the exciting dipole. At the same time, there is no contribution by the coupling from the next dipole, which has a reverse direction. The width of each microstrip feeding line w_f can be calculated using Equation (13) [40].

$$z_0 = \frac{87}{\sqrt{\varepsilon_r + 1.41}} \ln\left(\frac{5.98 \times h}{0.8 \times w_f}\right) \tag{13}$$

where h is the height of the substrate, z_0 represents the characteristic impedance 50 Ω. In this work, the balance feeding method is employed. The top microstrip line has a width $w_{f1} = 3.5$ mm while the width of the bottom microstrip line is $w_{f2} = 5$ mm, The 50 Ω impedance point is usually located near the narrow tip of the PLPDA antenna. To achieve impedance bandwidth less than −10 dB for all elements in the array, a parametric sweep has been performed to change the width of the transmission line by creating a balun to balance the surface currents distribution between the two sides of the transmission line as described in [28]. These optimum values are obtained with the help of CST Microwave studio to obtain wider impedance bandwidth starting from 0.5 GHz to 6 GHz.

5. Simulation and Measurement Results

The proposed design has been fabricated and tested in the EMC laboratory at the University of West Bohemia, Faculty of Electrical Engineering. Furthermore, the fabrication process takes place with the help of an LPKF ProtoMat S100 CNC machine. The utilized structure is epoxy FR-4 with relative permittivity $\varepsilon_r = 4.3$, and loss tangent of $tan\delta$ = 0.025. The phototype of the fabricated design is shown in Figure 11.

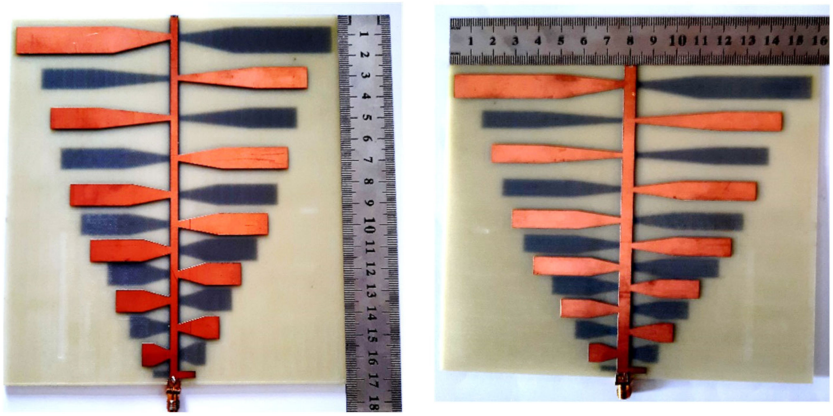

(**a**) (**b**)

Figure 11. The prototype of the proposed design: (**a**) front view; (**b**) back view.

5.1. S11-Parameter

The reflection coefficient of the proposed design has been measured using the RIGOL DSA875 Spectrum Analyzer (9 kHz–7.5 GHz) with directional couplers (RIGOL VB 1032 and RIGOL VB 2032), as shown in Figure 12a. These two directional couplers are utilized simultaneously to cover the band up to 8 GHz (RIGOL VB 1032 (0.1–3.2 GHz) and RIGOL VB 2032 (2 to 8 GHz)). Figure 12b shows the simulated and measured return losses. It can be seen that the design offers a wide impedance bandwidth of 0.55–6 GHz in both simulation and measurement results.

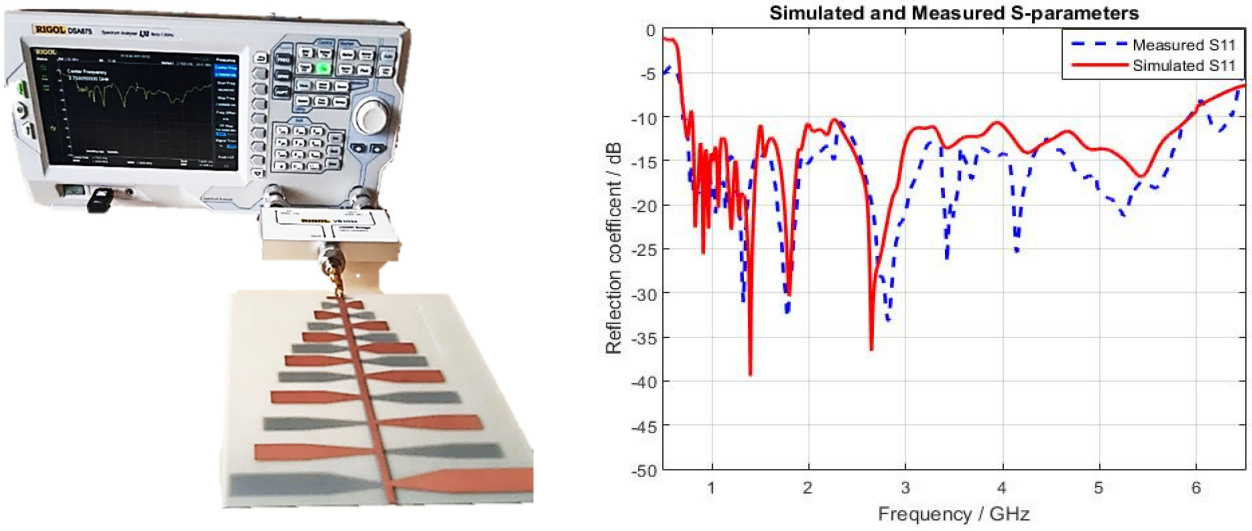

(**a**) (**b**)

Figure 12. (**a**) The reflection coefficient measurement setup of the proposed structure; (**b**) simulated and measured return losses versus frequency.

5.2. Surface Current Distribution

The surface current distribution is the best way to take a deep sight of the structure's behavior, and fortunately, this property exists in the simulation of CST Microwave studio software. Figure 13 demonstrates the surface current distribution at various frequency bands. The active region's transition from the large dipoles to the smaller ones coincides with the resonance frequency transition. The active region's smooth and continuous transition will reflect high gain and radiation pattern stability.

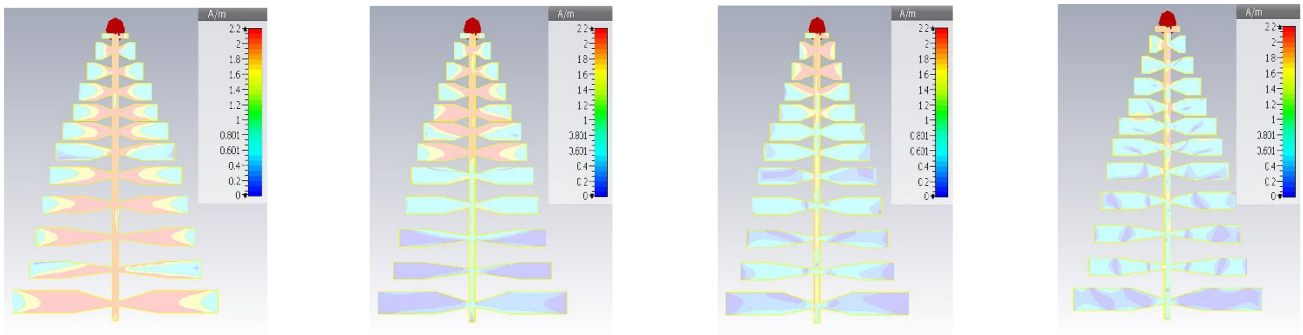

(**a**) (**b**) (**c**) (**d**)

Figure 13. Surface current distribution at: (**a**) 0.7 GHz; (**b**) 1.2 GHz; (**c**) 2.2 GHz; (**d**) 4.5 GHz.

5.3. Radiation Pattern

EMC chamber at the University of West Bohemia was utilized for radiation pattern and gain measurements, as shown in Figure 14. The proposed antenna is rotated around its axle 360° in both vertical and horizontal directions to achieve the results of the E-plane and H-plane, respectively. The simulated and measured radiation patterns in both the E- plane and H-plane are shown in Figures 15 and 16, respectively. Furthermore, the measured radiation patterns in both planes are agreeable with the simulated results from CST Microwave studio. The direction of the main lobe is at 90° for both elevation and azimuth plane. The back lobe of the azimuth plane is prominent at low frequencies and decreases gradually with high frequencies. The radiation pattern deterioration is clearly observed at high-frequency bands in both E-field and H-field presented in Figures 15 and 16, respectively [42].

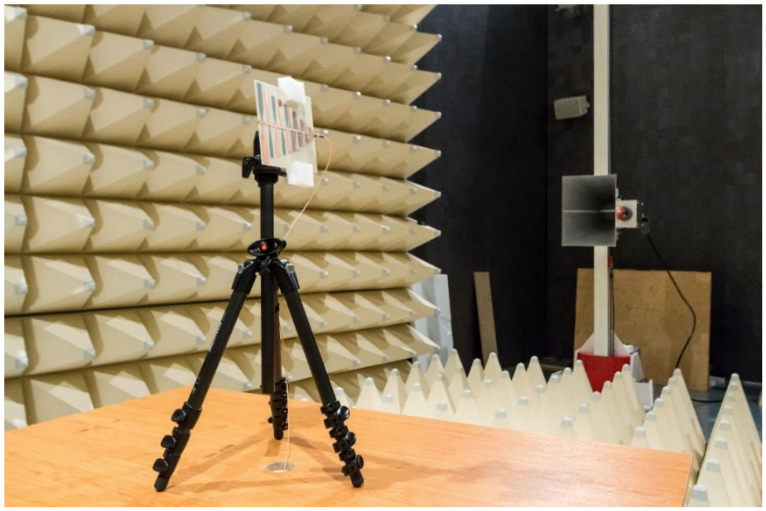

Figure 14. Radiation pattern setup for the proposed antenna inside EMC chamber.

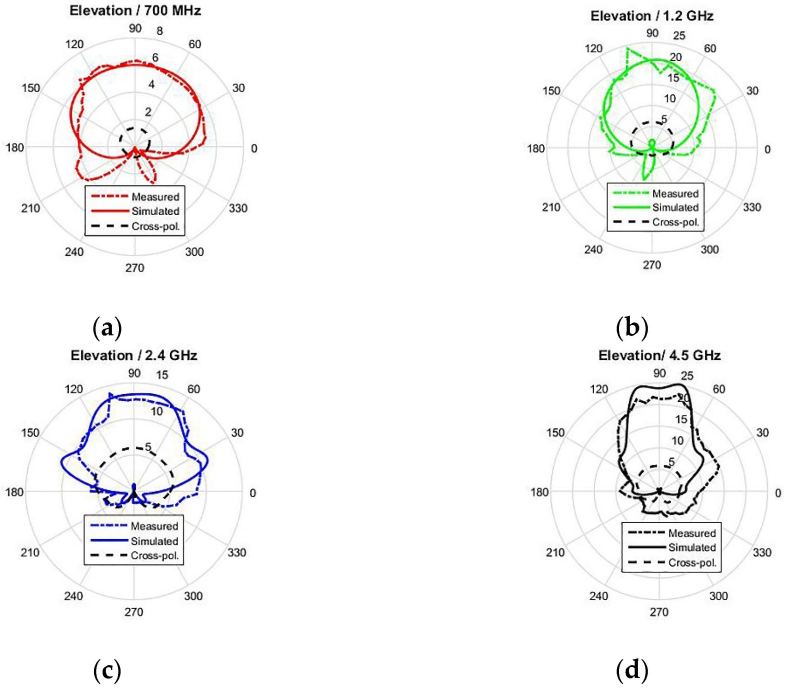

Figure 15. E-plane radiation pattern: (**a**) 0.7 GHz; (**b**) 1.2 GHz; (**c**) 2.2 GHz; (**d**) 4.5 GHz.

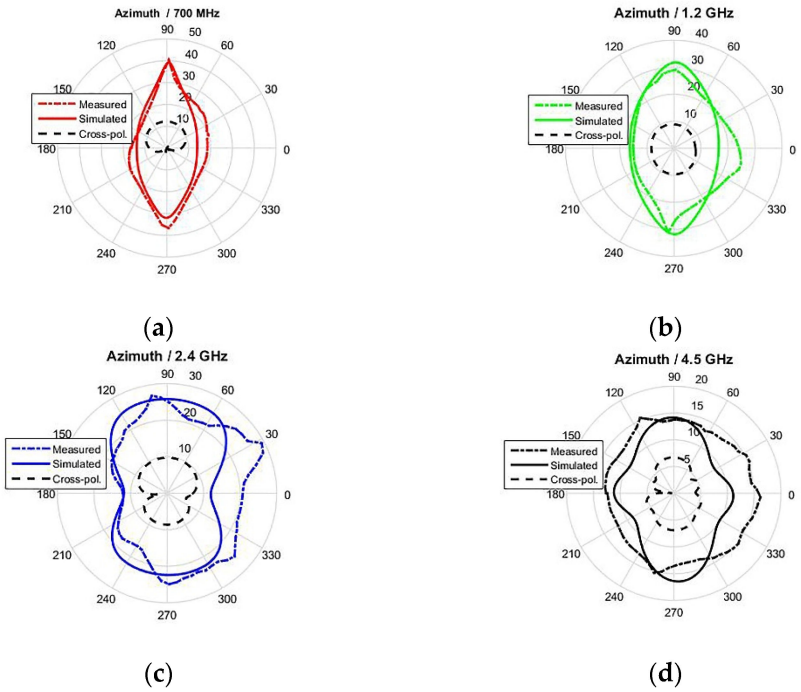

Figure 16. H-plane radiation pattern at: (**a**) 0.7 GHz; (**b**) 1.2 GHz; (**c**) 2.2 GHz; (**d**) 4.5 GHz.

5.4. Axial Ratio, Co and Cross-Polarization

One of the important parameters in designing a reference antenna is the Co-polarization (desired radiation) and Cross-polarization (orthogonal to the desired radiation) of the radiation pattern in both azimuth and elevation planes. The EMC reference antenna is required to be linearly polarized in the design. However, a slight difference in behaviors will appear from the designers' intentions. For instance, even the log-periodic dipole array antenna that uses opposite dipoles arrangement to provide smooth phase transportation between the elements shows an elliptical polarization. Furthermore, unwanted radiation will show up when the phase is not in the main element (cross-polarization), and this part cannot be eliminated. Instead, it could be minimized with the proper design. According to the EMC applications, the acceptable limit of cross-polarized rejection ratio is (14 dB to 20 dB) [43]. According to EMC standards, the cross-polarized in both E-plane and H-plane for the proposed antenna have been satisfied.

The term axial ratio (AR) demonstrates the type of polarization, whether circular, elliptical, or linear. The axial ratio of the circular polarization pounces between 0 and 3 dB, the AR of elliptical polarization is higher than 3 dB, and finally, the linear polarization will stand for AR going to infinity (theoretically). In fact, there is no practical/industrial norm for differentiating elliptically polarized antenna from linearly polarized antenna in terms of the axial ratio. Authors in [44] claimed the proposed design exhibits linear polarization with AR > 10 dB in planes ($\varphi = 0$, $\theta = 0$) and ($\varphi = 90$, $\theta = 0$) since linear polarization may be viewed as a special case of elliptical polarization. The phase difference between the two gain components was close to zero in the direction ($\theta = 0$), indicating linear polarization raised from the radiation pattern properties [45]. The proposed structure offered linear polarization with more than 20 dB AR except for some frequencies, as shown in Figure 17.

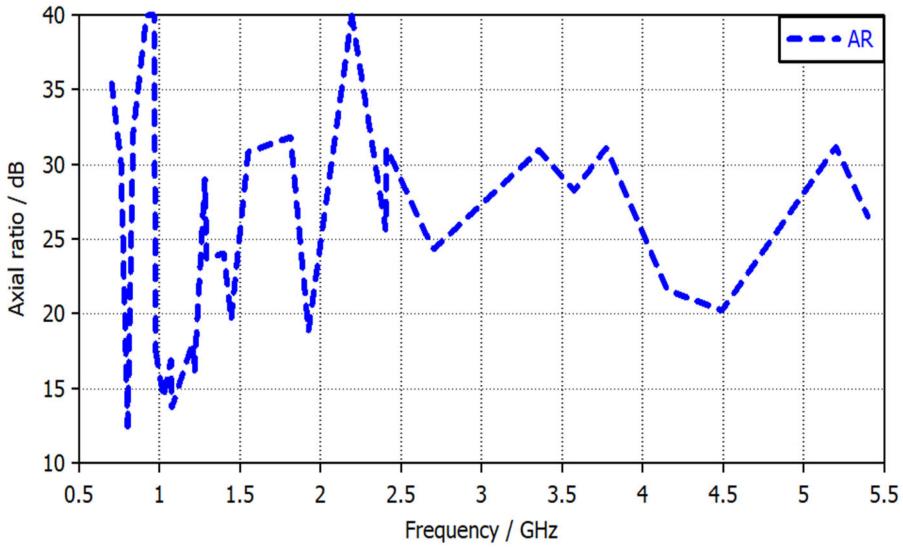

Figure 17. The simulated axial ratio in dB versus frequency.

5.5. Realized Gain and Antenna Factor

As we mentioned earlier, the bandwidth and the antenna factor are critical factors in designing the reference antenna. Wide bandwidth allows the detection of the EMI over a wide range of applications. At the same time, the antenna factor measures how much the structure is good to work as a reference antenna. The antenna factor is dedicated to finding out the incident field in space by knowing the received voltage. According to Equation (14), it is clear that the antenna factor is inversely proportional to the wavelength times the root square of the realized gain [16]. Equation (15) is used to calculate the antenna factor in (dB/m) from the realized gain of the antenna in (dBi).

$$AF = \frac{E_r}{V_r} = \frac{9.73}{\lambda \cdot \sqrt{G}} \tag{14}$$

$$AF = 20 \log \left[\frac{2\pi}{\lambda} \sqrt{\frac{2.4}{10^{(G(dBi)/10)}}} \right] \tag{15}$$

The simulated and measured realized gain (dBi) are depicted in Figure 18. Relatively small fluctuations in gain values (4.6–7) dBi reflect good behavior in antenna factor values (24–41) dBm^{-1}. Figure 19 shows the antenna factor versus frequency, while the antenna factor values are listed numerically for each frequency band in Table 2. It can be seen that the gain and, consequently, the antenna factor are in line with the typical values of a standard EMC antenna [46].

5.6. Comparison with the Literature Reviewed

In the last decade, several structures of PLPDA antenna were proposed to work as a reference antenna inside the chamber for EMC measurement, and these articles have used different techniques for size reduction and bandwidth enhancement. Table 3 lists the design specifications and achievements for these literature articles.

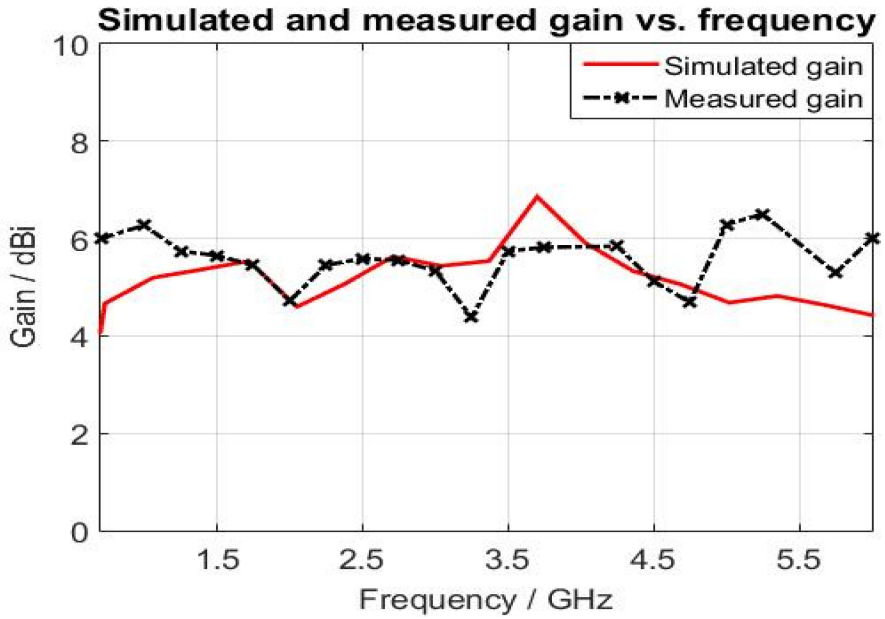

Figure 18. Presentation of the simulated and measured realized gain in dBi versus frequency.

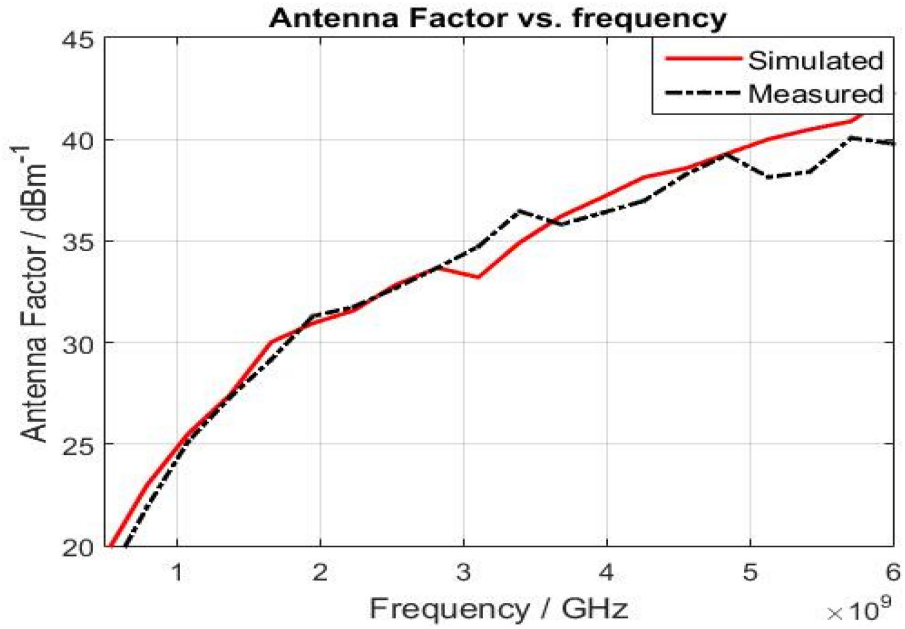

Figure 19. Presentation of the simulated and measured antenna factor in dBm^{-1} versus frequency.

Table 2. Illustration of optimum values of the antenna factor and corresponding gain versus frequency.

Freq./GHz	**0.7**	**1**	**1.5**	**2**	**2.5**	**3**	**3.5**	**4**	**4.5**	**5**	**5.5**	**6**
AF/dBm^{-1}	18	24.5	28.1	31.5	32.9	34.3	35.1	36.2	37.7	39.5	39.5	41.1
AG/dBi	7	5.7	5.6	4.7	5.2	5.4	6	6	5.5	4.7	5.4	4.6

Table 3. A comprehensive comparison between the proposed design and the literature papers.

Rf.	[27]	[28]	[29]	[30]	[31]	[32]	Our Work
Freq./GHz	(0.8–2.5)	(0.5–3)	(0.55–9)	(0.5–10)	(0.8–2.3)	(0.4–8)	(0.5–6)
FBW	103%	143%	177%	181%	96.7%	180%	170%
ε_r	4.3	4.3	3.5	3.5	4.3	4.3	4.3
τ	0.78	0.86	0.93	0.91	0.86	0.9	0.86
Gain/dBi	6.5	7–7.5	2.4–7.8	3–6	4.5–6.3	2.5–6.9	4.6–7
No.of dipoles	12	12	48	25	12	25	12
Size/λo	0.426 × 0.4	0.44 × 0.25	0.49 × 0.35	0.36 × 0.43	0.426 × 0.37	0.36 × 0.37	0.28 × 0.26
Feeding	Typical	Balanced	Typical	Typical	Optimized	Typical	Balanced
Application	EMC	EMC	EMC	EMC	EMC	EMC	EMC

It is worth mentioning that the relative bandwidth (FBW) presents the percentage of increased bandwidth and can be evaluated using Equations (16) and (17). Additionally, the size here is in terms of the wavelength that matches the lower frequency band (f_l).

$$FWB = \frac{f_h - f_l}{f_{av}} \times 100 \tag{16}$$

$$f_{av} = \frac{f_h + f_l}{2} \tag{17}$$

Table 3 illustrates the design specifications for several proposed designs that have been presented to serve as a reference antenna for EMC measurements inside the chamber [27–32]. The bandwidth enhancements and the size reduction are the main goals for all these works as they are controlled by the number of dipole elements and the spacing factor. For instance, [29] offers wide impedance bandwidth of about 8.5 GHz (FBW = 177%) with a fluctuating gain of 2.4–7.8 dBi, while it is required 48 elements with a size of 0.49 × 0.355 λ_L. Authors in [30] use the dual-band dipole element technique to achieve a wide bandwidth of 9.5 GHz (FBW = 181%), with a gain of 3–6 dBi, while it requires 25 elements with a size of 0.36 × 0.43 λ_L. On the other hand, our work aims to tackle bandwidth enhancement and size reduction goals. The proposed design uses a biconical dipole to obtain wide impedance bandwidth of 5.5 GHz (FBW = 170%), with a relatively low fluctuated gain of 4.6–7 dBi, and it requires only 12 elements based on a small size of 0.28 × 0.26 λ_L. Table 4 presents the miniaturization techniques that have been used in [29,30] and the size reduction percentage compared to our works. Moreover, the constant gain behavior in the whole frequency band reflects a good antenna factor compared to the commercial design.

Table 4. Comparison between the miniaturization techniques used in [29,30] and the proposed work.

Ref.	Size Reduction	Miniaturization Technique
[29]	27% and 20%	Using Hat loading and Top loading
[30]	40%	Using Dual-band dipoles
This work	50% and 50%	Using biconical dipoles

5.7. Comparison with the Commercial LPDA Antenna (HyperLOG® 7060)

A comprehensive comparison between the proposed structure and the commercial design HyperLOG® 7060 from the AARONIA AG website is listed in Table 5 [47]. HyperLOG® 7060 antenna has relative bandwidth of 158% with a size of 340 × 200 × 25 mm. On the other hand, the proposed antenna has better relative bandwidth of 170% with a compact size of 170 × 160 × 1.6 mm. Moreover, both commercial and proposed designs have an acceptable low variation gain related to the EMC applications and reflect good antenna factor values (AF).

Table 5. Comparison between the proposed antenna and commercial antenna.

Specifications	HyperLOG® 7060	Proposed Design
Dimensions/mm	340 × 200 × 25	170 × 160 × 1.6
Design	Logarithmic-periodic	Logarithmic-periodic
Substrate	-	FR-4
Weight/g	250	70
Gain/dBi	3.1–5.5	4.6–7
Frequency range/MHz	700–6000	500–6000
Antenna Factor $*^{(1)}$/dBm^{-1}	26–41	24.5–41.18
RF Connector	SMA Female	SMA Female
Picture		

$*^{(1)}$ frequency range from 0.7 GHz to 6 GHz.

The Antenna factor (AF) measures how much the proposed design is suitable to serve as a reference antenna by comparing the AF of the proposed structure with the standard AF. Unfortunately, none of the reviewed literature presents the antenna factor. In this work, the antenna factor of the reviewed literature, whose cover band is up to 6 GHz, and the proposed design were calculated from its given gain in dBi using Equation (15). The results are compared with the commercial Hyperlog 7060, as shown in Table 6. The AF of the proposed design has lower tolerance than the commercial Hyperlog 7060 due to the tiny fluctuations in the realized gain.

Table 6. Antenna factor comparison of the proposed design, the literature reviewed papers, and commercial design HyperLOG 7060.

Freq./GHz	AF [29]	AF [30]	AF [32]	Proposed Design	AF [HyperLOG 7060] [47]
0.5	20	20	22	18.1	–
1	23	25.5	29.5	24.5	26
1.5	27	28.5	30	28.1	29
2	30	31.5	30.5	31.5	31.5
2.5	32	33.5	32	32.9	33
3	34	36	34	34.3	35
3.5	35	37.5	35	35.1	36.5
4	36	39	36.5	36.2	37.25
4.5	37	40	37	37.78	37.75
5	37.9	41	38	39.5	38.5
5.5	39	41.5	38.5	39.54	40.5
6	40	42	40	41.18	41

It is worth mentioning the minimum 3 dB beamwidth of the proposed antenna is agreeable with the standard limits of the classical PLPDA in CISPR 16.1.2, as shown in Table 7. The minimum dimension of w can be calculated using Equation (18), where w is the minimum dimension of the line tangent to the DUT formed by the minimum 3 dB beamwidth (∅3dB), as shown in Figure 1.

$$w = 2 \times d \times \tan(0.5 \times \varnothing 3\text{dB}) \quad (18)$$

where, d is the minimum measurement distance between the reference antenna and the DUT and can be either 1 m, 3 m, or 10 m.

Table 7. Comparison between the minimum distance w in both CISPR 16.1.2 standard and proposed antenna at minimum measurement distance d = 1 m.

Frequency/GHz	$\varnothing_{3\ dB}$ CISPR 16.1.2/°	w of CISPR 16.1.2/m	$\varnothing_{3dB}$ Proposed Design/°	w of Proposed Design
1	60	1.15	112	2.95
2	55	1.04	141	4.28
4	55	1.04	55	1.04
6	55	1.04	46.4	0.85

6. Conclusions

A Compact size log-periodic dipole array antenna is designed, modeled, and fabricated. This design is dedicated to serving as a reference antenna for EMC measurement. The use of dipoles with biconical shapes rather than normal ones has reflected a size reduction of (50%) and bandwidth enhancement (relative bandwidth of 170%). Furthermore, the balance feeding method is deployed to obtain wideband impedance matching (from 0.5 GHz to 6 GHz). The compact size has given the freedom to change the measurement distance to 1.25 m in the case of a small DUT, and in this case, the illumination area will be 1.5 mm, which is suitable for most DUTs. A good value of the realized gain has been achieved with tiny fluctuation (4.6–7) dBi through the whole bandwidth with the help of an extra dipole. Calculating the antenna factor and comparing it with the standard result of the conventional LPDA antenna is a trusted investigation method to show the validity of the proposed design. For instance, an antenna factor (23–41) dB/m for the proposed design is compared to the antenna factor (26–41) dB/m for a commercial (0.7–6) GHz LPDA antenna (HyperLOG® 7060). Moreover, more investigations could be performed on this antenna for future work, such as the calibration and modeling of an equivalent circuit.

Author Contributions: Conceptualization, A.A.A. and Z.K.; methodology, A.A.A.; investigation, A.A.A. and Z.K.; resources, A.A.A. and Z.K.; writing—review and editing, A.A.A. and Z.K. All authors have read and agreed to the published version of the manuscript.

Funding: This research was supported by the Ministry of Education, Youth, and Sports of the Czech Republic under the project OP VVV Electrical Engineering Technologies with High-Level of Embedded Intelligence CZ.02.1.01/0.0/0.0/18_069/0009855 and by the project SGS-2021-005: Research, development, and implementation of modern electronic and information systems.

Institutional Review Board Statement: Not applicable.

Informed Consent Statement: Not applicable.

Data Availability Statement: Not applicable.

Conflicts of Interest: The authors declare no conflict of interest.

References

1. Abdulhameed, A.A.; Alhamdawee, E.M.; Hayder, I.M. Review of reconfigurable/UWB antenna for interweave cognitive radio applications. *Aust. J. Electr. Electron. Eng.* **2019**, *16*, 96–101. [CrossRef]
2. Bakr, M.S.; Alterkawi, A.B.A.; Gentili, F.; Bosch, W. Reconfigurable ultra-wide-band patch antenna: Cognitive radio. In Proceedings of the 2017 IEEE MTT-S International Microwave Workshop Series on Advanced Materials and Processes for RF and THz Applications (IMWS-AMP), Pavia, Italy, 20–22 September 2017; pp. 1–3.
3. Al-Yasir, Y.I.A.; Abdulkhaleq, A.M.; Parchin, N.O.; Elfergani, I.T.; Rodriguez, J.; Noras, J.M.; Abd-Alhameed, R.A.; Rayit, A.; Qahwaji, R. Green and Highly Efficient MIMO Transceiver System for 5G Heterogenous Networks. *IEEE Trans. Green Commun. Netw.* **2022**, *6*, 500–511. [CrossRef]
4. Jasim, A.M.; Al-Anbagi, H.N. A comprehensive study of spectrum sensing techniques in cognitive radio networks. In Proceedings of the 2017 International Conference on Current Research in Computer Science and Information Technology (ICCIT), Sulaymaniyah, Iraq, 26–27 April 2017; pp. 107–114.
5. Al-Anbagi, H.N.; Vertat, I. Cooperative Reception of Multiple Satellite Downlinks. *Sensors* **2022**, *22*, 2856. [CrossRef] [PubMed]

6. Das, A.; Chatterjee, D.; Bhattacharya, A.; Majumder, S.; Chakravarty, D.; Byabarta, N. Comparative study of different techniques to design ultra wideband antenna in cognitive radio. In Proceedings of the 2017 4th International Conference on Opto-Electronics and Applied Optics (Optronix), Kolkata, India, 2–3 November 2017; pp. 1–7.
7. Mohammed, A.A.; Alnahwi, F.M.; Abdullah, A.S.; Hameed, A.G.A.A. A compact monopole antenna with reconfigurable band notch for underlay cognitive radio applications. In Proceedings of the 2018 International Conference on Advance of Sustainable Engineering and its Application (ICASEA), Wasit-Kut, Iraq, 14–15 March 2018; pp. 25–30.
8. Abdulhameed, A.A.; Alnahwi, F.M.; Swadi, H.L.; Abdullah, A.S. A compact cognitive radio UWB/reconfigurable antenna system with controllable communicating antenna bandwidth. *Aust. J. Electr. Electron. Eng.* **2019**, *16*, 1–11. [CrossRef]
9. Tu, Y.; Al-Yasir, Y.I.A.; Ojaroudi Parchin, N.; Abdulkhaleq, A.M.; Abd-Alhameed, R.A. A Survey on Reconfigurable Microstrip Filter–Antenna Integration: Recent Developments and Challenges. *Electronics* **2020**, *9*, 1249. [CrossRef]
10. Abdulhameed, A.A.; Alnahwi, F.M.; Al-Anbagi, H.N.; Kubík, Z.; Abdullah, A.S. Frequency reconfigurable key-shape antenna for LTE applications. *Aust. J. Electr. Electron. Eng.* **2022**, 1–9. [CrossRef]
11. Al-Yasir, Y.I.A.; Ojaroudi Parchin, N.; Tu, Y.; Abdulkhaleq, A.M.; Elfergani, I.T.E.; Rodriguez, J.; Abd-Alhameed, R.A. A Varactor-Based Very Compact Tunable Filter with Wide Tuning Range for 4G and Sub-6 GHz 5G Communications. *Sensors* **2020**, *20*, 4538. [CrossRef] [PubMed]
12. Kubík, Z.; Skála, J. Shielding effectiveness measurement and simulation of small perforated shielding enclosure using FEM. In Proceedings of the 2015 IEEE 15th International Conference on Environment and Electrical Engineering (EEEIC), Rome, Italy, 10–13 June 2015; pp. 1983–1988.
13. Kim, K.-C.; Choi, B.J.; Jung, S.W.J. Characteristics of the Sleeve Dipole Antenna Used for EMC Applications. *IEEE Access* **2020**, *8*, 86957–86961. [CrossRef]
14. Bang, J.; Han, C.; Jung, K.; Choi, J. High-frequency performance improvement of LPDA for EMC/EMI measurements. In Proceedings of the 2020 International Symposium on Antennas and Propagation (ISAP), Osaka, Japan, 25–28 January 2021; pp. 621–622.
15. Kawakami, H.; Tanioka, M.; Wakabayashi, R. Circularly polarized log periodic dipole antennas. In Proceedings of the 2020 International Applied Computational Electromagnetics Society Symposium (ACES), Monterey, CA, USA, 27–31 July 2020; pp. 1–2.
16. Ivšić, B.; Friščić, F.; Dadić, M.; Muha, D. Design and analysis of Vivaldi antenna for measuring electromagnetic compatibility. In Proceedings of the 2019 42nd International Convention on Information and Communication Technology, Electronics and Microelectronics (MIPRO), Opatija, Croatia, 20–24 May 2019; pp. 491–495.
17. Gerber, M.; Odendaal, J.W.; Joubert, J. DRGH antenna with improved gain and beamwidth performance. *IEEE Trans. Antennas Propag.* **2019**, *68*, 4060–4065. [CrossRef]
18. Jiang, J.; Pan, S.; Wang, S.; Li, G. Miniaturization design of VHF broadband directional radiation TEM horn antenna. In Proceedings of the 2020 International Conference on Microwave and Millimeter Wave Technology (ICMMT), Shanghai, China, 20–23 September 2020; pp. 1–3.
19. Mallahzadeh, A.; Pazoki, R.; Karimkashi, S. A new UWB skeletal antenna for EMC applications. In Proceedings of the 2007 International Symposium on Microwave, Antenna, Propagation and EMC Technologies for Wireless Communications, Hangzhou, China, 16–17 August 2007; pp. 543–546.
20. Hacene, Y.; Shuguo, X. Study of a novel ultra-wideband monopole antenna for EMC measurement applications. In Proceedings of the 2012 6th Asia-Pacific Conference on Environmental Electromagnetics (CEEM), Shanghai, China, 6–9 November 2012; pp. 393–395.
21. Tziris, E.N.; Lazaridis, P.I.; Zaharis, Z.D.; Cosmas, J.P.; Mistry, K.K.; Glover, I.A. Optimized Planar Elliptical Dipole Antenna for UWB EMC Applications. *IEEE Trans. Electromagn. Compat.* **2019**, *61*, 1377–1384. [CrossRef]
22. Kuhn, W.; Peterson, G.; Welch, J. Broadband Antenna Probe for Microwave EMC Measurements. In Proceedings of the 2018 IEEE 27th Conference on Electrical Performance of Electronic Packaging and Systems (EPEPS), San Jose, CA, USA, 14–17 October 2018; pp. 199–201.
23. Abdulhameed, A.A. Circular slotted monopole printed antenna with grounded stub WLAN band-notch for UWB applications. *Aust. J. Electr. Electron. Eng.* **2017**, *14*, 59–63. [CrossRef]
24. Abdulhameed, A.A.; Kubík, Z. Investigation of Broadband Printed Biconical Antenna with Tapered Balun for EMC Measurements. *Energies* **2021**, *14*, 4013. [CrossRef]
25. Alnahwi, F.M.; Abdulhameed, A.A.; Swadi, H.L.; Abdullah, A.S. A planar integrated UWB/reconfigurable antenna with continuous and wide frequency tuning range for interweave cognitive radio applications. *Iran. J. Sci. Technol. Trans. Electr. Eng.* **2019**, *44*, 729–739. [CrossRef]
26. Casula, G.A.; Maxia, P.; Mazzarella, G.; Montisci, G. Design of a printed log-periodic dipole array for ultra-wideband applications. *Prog. Electromagn. Res. C* **2013**, *38*, 15–26. [CrossRef]
27. Limpiti, T.; Chantaveerod, A.Y. Design of a printed log-periodic dipole antenna (LPDA) for 0.8–2.5 GHz band applications. In Proceedings of the 2016 13th International Conference on Electrical Engineering/Electronics, Computer, Telecommunications and Information Technology (ECTI-CON), Chiang Mai, Thailand, 28 June–1 July 2016; pp. 1–4.
28. Yu, L.; Chai, S.; Huang, H.; Ding, L.; Xiao, K.; Zhao, F. A printed log-periodic dipole antenna with balanced feed structure. In Proceedings of the 2016 Progress in Electromagnetic Research Symposium (PIERS), Shanghai, China, 8–11 August 2016; pp. 2035–2038.

29. Kyei, A.; Sim, D.-U.; Jung, Y.-B. Compact log-periodic dipole array antenna with bandwidth-enhancement techniques for the low frequency band. *IET Microw. Antennas Propag.* **2017**, *11*, 711–717. [CrossRef]
30. Anim, K.; Jung, Y.-B. Shortened log-periodic dipole antenna using printed dual-band dipole elements. *IEEE Trans. Antennas Propag.* **2018**, *66*, 6762–6771. [CrossRef]
31. Mistry, K.K.; Lazaridis, P.I.; Zaharis, Z.D.; Xenos, T.D.; Tziris, E.N.; Glover, I.A. An optimal design of printed log-periodic antenna for L-band EMC applications. In Proceedings of the 2018 IEEE International Symposium on Electromagnetic Compatibility and 2018 IEEE Asia-Pacific Symposium on Electromagnetic Compatibility (EMC/APEMC), Suntec City, Singapore, 14–18 May 2018; pp. 1150–1155.
32. Mistry, K.K.; Lazaridis, P.I.; Ahmed, Q.; Zaharis, Z.D.; Loh, T.H.; Chochliouros, I.P. A printed LPDA antenna with improved low frequency response. In Proceedings of the 2020 XXXIII General Assembly and Scientific Symposium of the International Union of Radio Science, Rome, Italy, 29 August–5 September 2020; pp. 1–4.
33. Kubacki, R.; Czyżewski, M.; Laskowski, D. Enlarged Frequency Bandwidth of Truncated Log-Periodic Dipole Array Antenna. *Electronics* **2020**, *9*, 1300. [CrossRef]
34. Wu, Q.; Ding, X.; Su, D. A compact dipole antenna with curved reflector for 1.0–4.2 GHz EMC measurement. *IEEE Trans. Electromagn. Compat.* **2015**, *57*, 1289–1297. [CrossRef]
35. *CISPR16-1-2*; Specification for Radio Disturbance and Immunity Measuring Apparatus and Methods—Part 1–2: Radio Disturbance and Immunity Measuring Apparatus-Ancillary Equipment-Conducted Disturbances. International Electrotechnical Commission: Geneva, Switzerland, 2006.
36. Microwave Vision Group. Considerations in EMI Antenna Design. Available online: http://www.interferencetechnology.com/wp-content/uploads/2021/02/Whitepaper-EMC-Considerations-in-EMI-Antenna-Design.pdf (accessed on 8 August 2022).
37. Isbell, D. Log periodic dipole arrays. *IRE Trans. Antennas Propag.* **1960**, *8*, 260–267. [CrossRef]
38. DuHamel, R.; Isbell, D. Broadband logarithmically periodic antenna structures. In Proceedings of the 1958 IRE International Convention Record, New York, NY, USA, 21–25 March 1966; pp. 119–128.
39. Carrel, R. The design of log-periodic dipole antennas. In Proceedings of the 1958 IRE International Convention Record, New York, NY, USA, 21–25 March 1966; pp. 61–75.
40. Balanis, C.A. *Antenna Theory: Analysis and Design*; John Wiley & Sons: Hoboken, NJ, USA, 2015.
41. Dassault Systemes. *CST Computer Simulation Technology AG (2016)*; Dassault Systemes: Darmstadt, Germany, 2014.
42. Vieira, G.C. *Log-Periodic Dipole Antennas in Printed Circuit Technology*; Instituto Superior Tecnico: Lisboa, Portugal, 2018.
43. Alexander, M.; Salter, M.; Gentle, D.; Knight, D.; Loader, B.; Holland, K. *Calibration and Use of Antennas, Focusing on EMC Applications*; National Physical Laboratory: Teddington, UK, 2004.
44. Patre, S.R.; Singh, S.; Singh, S.P. Effect of dielectric substrate on performance of planar trapezoidal toothed log-periodic antenna. In Proceedings of the 2013 Students Conference on Engineering and Systems (SCES), Allahabad, India, 12–14 April 2013; pp. 1–4.
45. Kim, J.I.; Safaai-Jazi, A.J. Log-periodic loop antennas with high gain and linear polarization. *Microw. Opt. Technol. Lett.* **2000**, *27*, 66–68. [CrossRef]
46. McLean, J.; Sutton, R.; Hoffman, R.J. *Interpreting Antenna Performance Parameters for EMC Applications: Part 3: Antenna Factor*; TDK RF Solutions Inc.: Cedar Park, TX, USA, 2004.
47. Shop, A. HyperLOG® 7060. Available online: https://aaronia-shop.com/products/broadband-antenna-hyperlog7060 (accessed on 8 August 2022).